Author's copy of paper published in the *Journal of Infrastructure Systems*, June 24, 2022

Modeling regional and local resilience of infrastructure networks following disruptions from natural hazards

Dylan Sanderson[1]*; Daniel Cox[2]; Andre R. Barbosa[3]; John Bolte[4]

[1]Ph.D. Student, School of Civil and Construction Engineering, Oregon State University, Corvallis, Oregon, United States. https://orcid.org/0000-0002-4443-7074

[2]CH2M Hill Professor in Civil Engineering, School of Civil and Construction Engineering, Oregon State University, Corvallis, Oregon, United States

[3]Associate Professor, School of Civil and Construction Engineering, Oregon State University, Corvallis, Oregon, United States. https://orcid.org/0000-0003-4547-531X

[4]Department Head, Biological and Ecological Engineering, Oregon State University, Corvallis, Oregon, United States. https://orcid.org/0000-0003-0059-4219

*corresponding author: sanderdy@oregonstate.edu

Abstract

This paper presents a framework to evaluate the regional and local resilience of infrastructure networks following disruptions from natural hazards. Herein, the regional resilience of a network relates to the accessibility of a community within a larger network, whereas the local resilience concerns the ability of a network to provide its intended service within the boundaries of a community. Using this framework, a methodology is developed to demonstrate its application to a road and highway transportation network disrupted by ground shaking and inundation under a Cascadia Subduction Zone earthquake and tsunami scenario. The regional network extents comprise the entire coast of the state of Oregon, United States of America. Embedded within this regional network are 18 local networks associated with coastal communities. Regional and local connectivity indices are defined to identify the initial damage and then track the post-disaster recovery of the transportation network, *i.e.*, evaluate the network resilience. Results identify the attributes that lead to a regionally or locally resilient network and highlight the importance of considering local infrastructure networks embedded within larger regional networks. It is shown that without regional considerations, the time to recover may be severely underpredicted. The methodology is further used as a decision support tool to demonstrate how mitigation options impact the transportation network's resilience. The importance of strategically considering mitigation options is emphasized as some communities see significant reductions in time to recover, whereas others see little to no improvement.

Keywords

Community resilience; natural hazards; infrastructure networks; multiple scales

Introduction

Infrastructure networks, such as electric power, transportation, and communication, are essential for community function and resilience planning (OSSPAC, 2013; NIST, 2016); however, these networks are often evaluated without considerations given to the larger regional network that they are embedded within. That is, the network's spatial boundaries are limited to the community's spatial boundaries. Infrastructure networks do, however, span multiple spatial scales ranging from global accessibility, *e.g.,* ship and airplane traffic, to traversing communities and neighborhoods, *e.g.,* local roads and walking trails. Further, depending on the type of infrastructure network, different services can be identified. For example, a transportation network may be used to connect people to food sources (Coveney and O'Dwyer, 2009), health resources (Zhang *et al.*, 2018), or post-disaster relief (Horner and Widener, 2011). Hazards, both natural and anthropogenic, can cause damage to network components, which translate to larger system disruptions and ultimately limit the ability of a network to perform it's intended service (Crucitti *et al.*, 2004; Buldyrev *et al.,* 2010).

When considering infrastructure networks under disruption from hazards, multiple spatial scales are of importance (Thacker *et al.,* 2017; Zhang and Alipour, 2020). For example, following a network disruption, a community may be accessible at the regional scale, *e.g.,* goods can reach the community boundaries; however, if the local network is in poor condition, then these goods cannot be distributed throughout the community. Conversely, if the local network of a community is in good condition following a disaster, but this network is not accessible to the rest of the region, then goods cannot be transported to the community, which in turn cannot be distributed throughout the local network. Thus, the extent to which a community is regionally or locally accessible is of importance.

The purpose of this paper is to present a generalized framework to simultaneously assess the regional and local resilience of infrastructure networks following disruptions from natural hazards. This framework is used to identify the attributes that lead to the regional and local resilience of networks, to demonstrate the necessity of considering local networks embedded within a larger, regional-scale network, and to evaluate the impact of alternative mitigation options on network resilience. The generalized framework is intended to be expandable across infrastructure network systems; however, in this paper a methodology is developed to demonstrate how the framework can be applied to a road and highway transportation network subject to the multi-hazard earthquake and tsunami threat posed by the Cascadia Subduction Zone.

The remainder of this paper is organized as follows: Section 2 outlines the framework in a generalized manner and draws on examples in the literature of how this can be applied across different infrastructure systems; Section 3 develops a methodology demonstrating how the framework can be applied to a road and highway transportation network; Section 4 presents results from the previous section and shows how the framework can be used to evaluate mitigation options; Section 5 presents a discussion of this work and identifies limitations; and lastly, Section 6 summarizes the conclusions.

General Framework

Figure 1 shows the general framework developed to assess the regional and local resilience of infrastructure networks and is broken up into three primary steps. The first step consists of organizing and collecting data. Using network and hazard data, damages to the network components are then evaluated in step 2. The damages result in changes to network component functionality, which then determine how the network performs as a system in step 3. Regional and local resilience metrics are defined and tracked here, from which the multi-scale resilience can be evaluated.

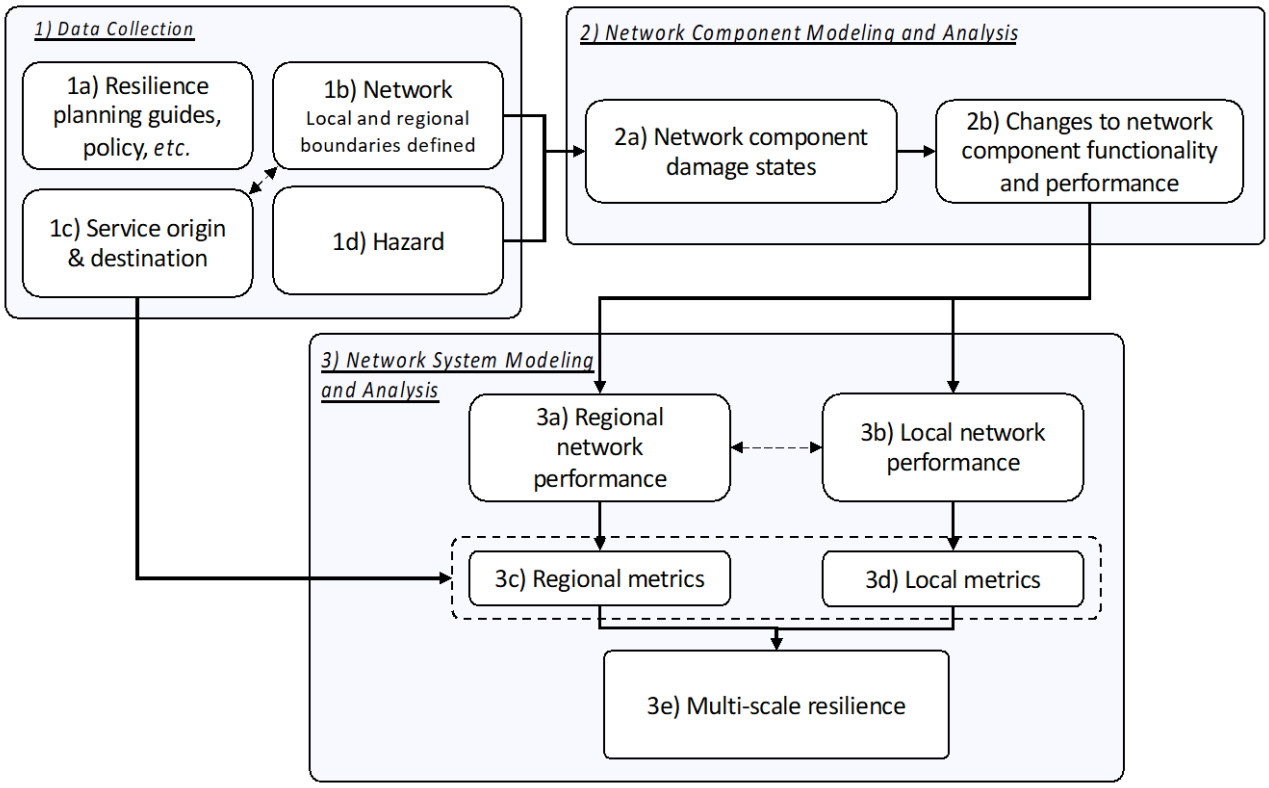

Fig. 1. Framework for assessing the regional and local resilience of infrastructure networks.

The first step, data collection, consists of gathering (1a) resilience planning guides and policy, (1b) network data, (1c) service information, and (1d) hazard data. Resilience planning guides and policies inform the overall analysis and can aide in identifying hazards present within a geographic region, metrics that can be tracked, or services that infrastructure networks provide (SPUR, 2009; OSSPAC, 2013; NIST, 2016; New York City Emergency Management, 2019).

Identifying the network (step 1b) consists of specifying an infrastructure network to consider and delimitating local and regional network boundaries. The latter is necessary to consider the problem under a multi-scale lens. For example, transportation networks may have regional boundaries connecting state to state (Omer *et al.*, 2013), or local boundaries concerning

accessibility within cities (Dong *et al.,* 2016; Dong *et al.,* 2020). Further, different spatial boundaries impact ownership of infrastructure components. For example, a state may be responsible for bridges along a highway, whereas cities are responsible for bridges within city boundaries.

Here, the term *service* refers to the service that the infrastructure network was originally intended to do (step 1c). Infrastructure networks can perform multiple services. For example, a transportation network can be used to move people from their place of residence to places that provide health assistance (Zhang *et al.,* 2018). Similarly, the same transportation network may be used to provide accessibility from places of residence to places of work (Omer *et al.,* 2011). As such, identifying the service of a network also consists of identifying origins and destinations that relate to this service. The service origin and destination are dependent on the network and vice versa.

The hazard (step 1d) consist of defining an event that inhibits the network from performing it's intended service (Ouyang, 2014; Faturechi and Miller-Hooks, 2015; Sun *et al.,* 2018). Hazards can be either natural, such as earthquakes (Chang and Nolima, 2001; Shiraki *et al.*, 2007; Guo *et al.*, 2017; Ishibashi *et al.,* 2021) and hurricanes (Horner and Widener, 2011; Zou and Chen, 2020); or anthropogenic, such as intentional attacks (Wu *et al.,* 2007). In the context of natural hazards, these hazards can often consist of multiple hazards which, if applicable, add an extra-dimension to the problem (Kappes *et al.*, 2012).

Step 2 of the framework, network component modeling and analysis, is the result of the hazard impacting the network. In the context of natural hazards, the hazard and network components are often combined via the use of fragility models (FEMA, 2013; Cavalieri *et al.,* 2014; Kakder and Argyroudis, 2014; FEMA, 2015; Gidaris *et al.*, 2017). The use of fragility models results in the probability of network components being in or exceeding a damage state (step 2a). The damage states subsequently inform changes to the network component functionality and performance (step 2b). The component functionality influences the component performance. In the case of transportation networks, performance may correspond to an increase in travel time along roads and bridges (Shiraki *et al.,* 2007), whereas in power networks may correspond to component failure (Ouyang and Dueñas-Osorio, 2014; Johnson *et al.*, 2020).

The entire network is then considered as a system in step 3. The performance of a network as a system depends upon both the individual component performance and network topology (Zhang *et al.,* 2015). This system performance can further be evaluated at multiple scales, hence both the regional and local network performance steps 3a and 3b. The arrow between these steps identifies interdependencies between the two. Based on the network and service that are being considered, there may be either a one-way dependence, *e.g.,* the local network depends on the regional network, or there may be a two-way dependence, *e.g.*, the local and regional networks depend upon each other. Regional and local metrics are identified (steps 3c and 3d) to evaluate the performance of the network under multiple scales. The service origin and destination aid in identifying the local

and regional metrics (Logan and Guikema, 2020). Last, the regional and local metrics are used to inform the multi-scale resilience of the network (step 3e).

Methods applied to a Transportation Network

A methodology was developed to demonstrate how the generalized framework can be applied to a road and highway transportation network under disruption from earthquake and tsunami hazards. This section follows steps 1 and 2 of the framework shown in Figure 1.

Hazard, Network, and Service Identification

The North American Pacific Northwest is subject to the rupture of the Cascadia Subduction Zone (CSZ), which can result in both strong earthquake ground shaking and tsunami inundation. The last full rupture of the CSZ occurred in 1700 and is estimated to have had a moment magnitude between 8.7 and 9.2. Further, some studies have estimated a 7-11 percent probability of a full-margin rupture to occur between 2010-2060 (Goldfinger *et al.*, 2012). Local studies to characterize the hazard associated with the CSZ have resulted in probabilistic hazard maps (Gonzàlez *et al.,* 2009; Park *et al.*, 2017); whereas at the regional scale, the hazard has been characterized based on moment-magnitude. In this work, scenario-based hazard maps associated with the M9.0 earthquake and corresponding large, or "L", tsunami were used (Madin et al., 2013; Priest et al., 2013) because this formed the basis of the Oregon Resilience Plan (OSSPAC, 2013). In the future, a probabilistic rather than a scenario-based approach could be considered as suggested by one of the reviewers. While a probabilistic seismic and tsunami hazard analysis (PSTHA) exists for a single community at Seaside, OR (Park *et al.*, 2017) and has been used for several risk-based damage studies (*e.g.*, Park *et al*., 2019; Sanderson *et al.*, 2021), there currently exist no PSTHA for the entire Pacific Northwest.

The regional highway transportation network considered is shown in Figure 2 and stretches from the California to Washington state borders in the north-south direction and from the Pacific coast to Interstate 5 in the east-west direction. The entire transportation network consists of 2,644 km of roads. Highways were prioritized according to a tiered approach with Tier 1 being a backbone that allows access to most major population centers, and Tier 3 providing access to all coastal communities (OSSPAC, 2013). The tiered structure of the transportation network is shown in Figure 2 and was used in this work when prioritizing restoration of highway components.

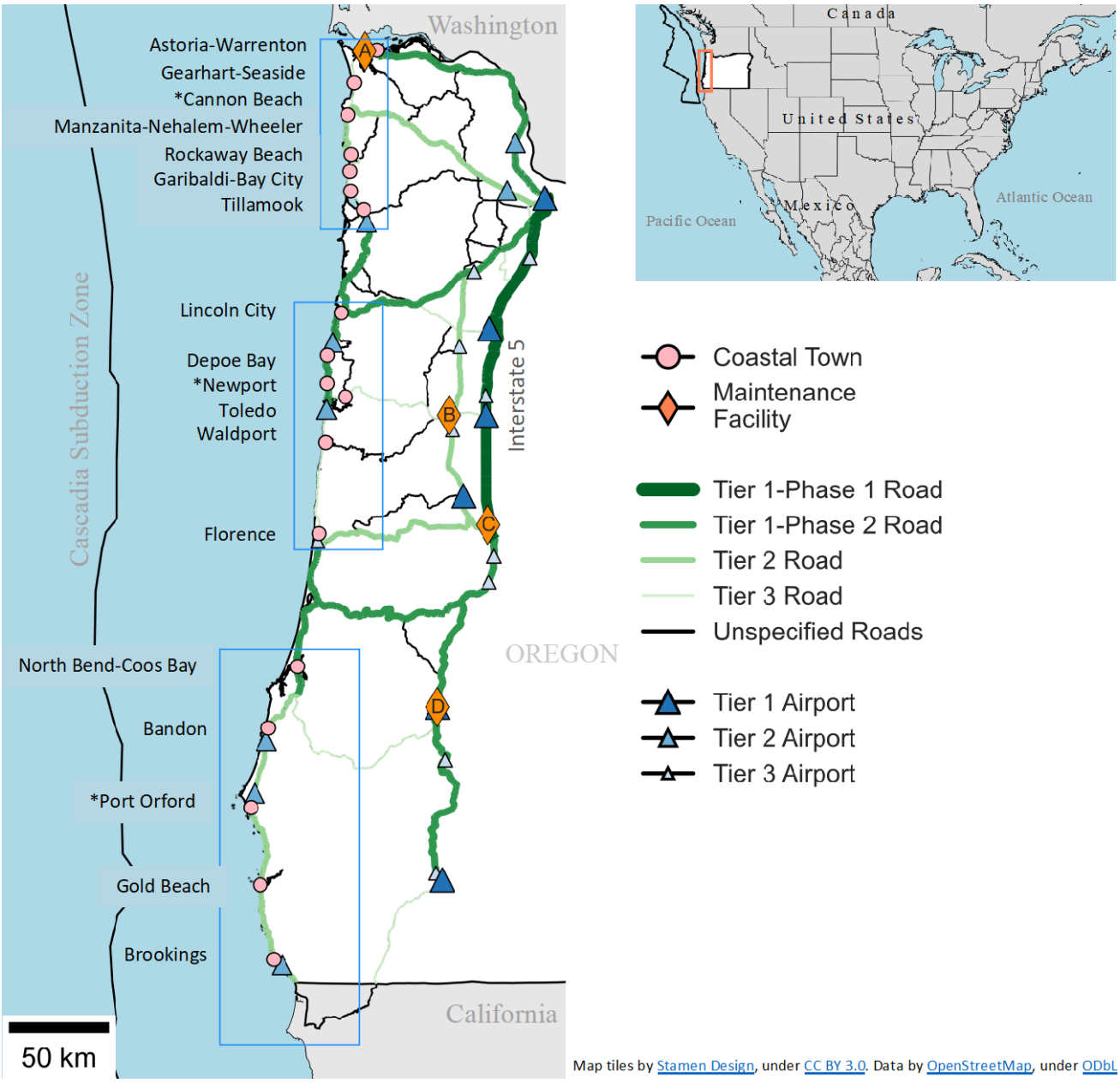

Fig. 2. Regional highway transportation network showing location of coastal communities, maintenance facilities, airports, and highway tiers.

It was assumed that the role of the transportation network is to provide post-disaster aid to communities, and the location of airports are used as a proxy for supply sources. Thus, in relation to the framework in Figure 1, airports were identified as the service origins, whereas coastal communities were identified as the service destinations. A total of 29 airports were considered and grouped into three tiers as shown in Figure 2. If an airport was located outside of the transportation network, the nearest

node on the network is used as a representative point. It should be highlighted that other services such as fuel, food, health, or access to large metropolitan areas could be identified, although these are not considered in the illustrative example shown here.

Furthermore, locations of transportation maintenance facilities are shown in Figure 2. Each coastal town is located within the jurisdiction of a single facility, and it was assumed that the reconstruction of local roads are dependent on the communities' accessibility to their respective maintenance facility. The maintenance facilities are labeled *A, B, C,* and *D.*

Within the regional network, 18 coastal communities were considered and are shown as pink dots in Figure 2 and summarized in Table 1. The 18 coastal communities were grouped into north, central, and south coast. The north coast communities are closer to metropolitan areas whereas the south coast is considered more rural. Local network boundaries were delimited by the urban growth boundary of each community, and some coastal towns that are near to others, such as Astoria-Warrenton and Gearhart-Seaside, were considered as one community for simplicity. The communities range in population from 954 people (Port Orford) to 25,881 people (North Bend-Coos Bay) (US Census Bureau, 2019). On average, the population of all 18 communities is 6,234 people and there are 90.5 km of roads within each community. Information in Table 1, such as population and median income is supplied to provide a sense of the size of each community but is not used further in this study. Figure 3 shows the local networks for three of the coastal communities: Cannon Beach, Newport, and Port Orford. The extent of tsunami inundation and the location of bridges and airports are shown.

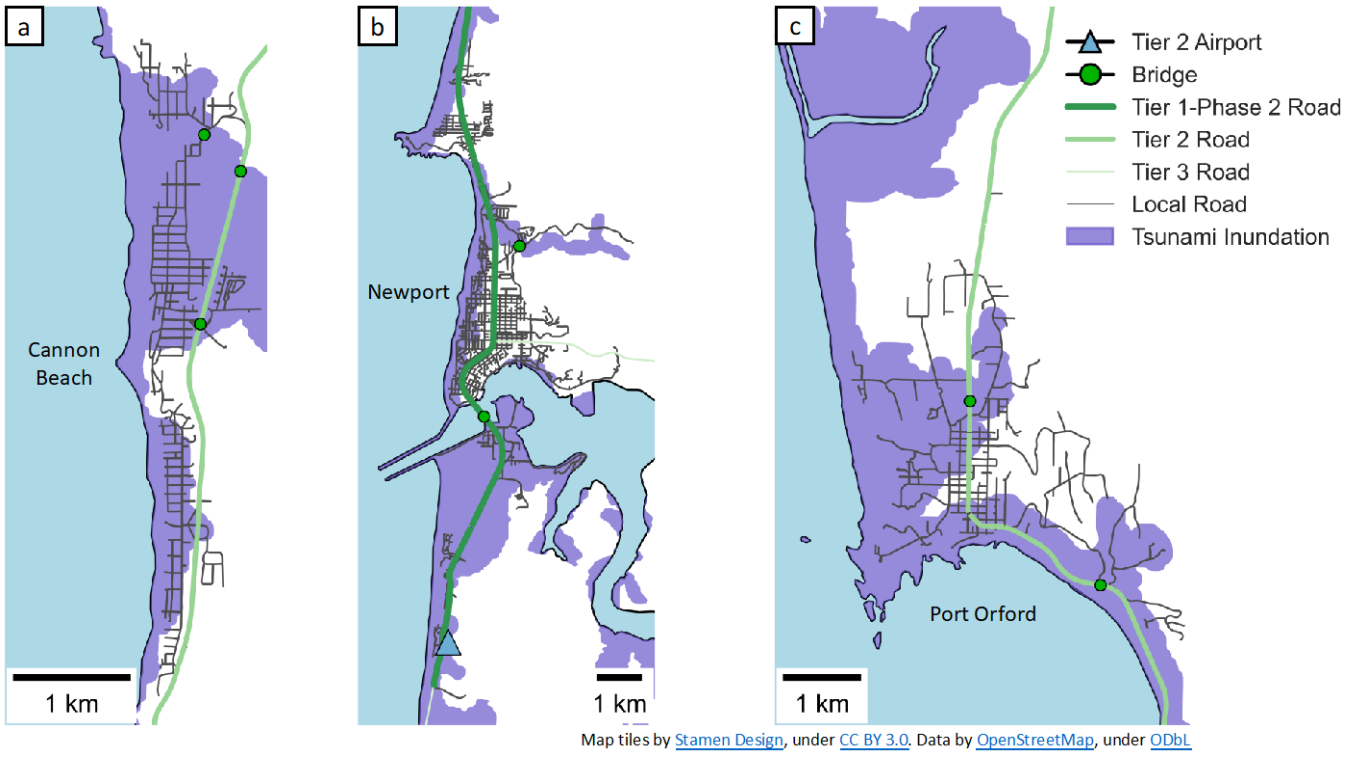

Fig. 3. Example of three local networks for (a) Cannon Beach, (b) Newport, and (c) Port Orford.

Table 1: Sociodemographic and transportation network summary for each coastal community and entire coast.

Community	Population	Median Annual Income	Number of nodes	Number of edges	Length Roads (km.)	Assigned Maintenance Facility
Astoria-Warrenton	15,385	$52,195	1,290	1,558	208.6	A
Gearhart-Seaside	8,382	$51,729	710	885	103.0	A
Cannon Beach	1,491	$50,846	323	392	38.1	A
Manzanita-Nehalem-Wheeler	1,105	$49,922	449	555	62.3	A
Rockaway Beach	1,166	$45,781	448	545	52.5	A
Garibaldi-Bay City	2,472	$53,064	354	412	43.0	A
Tillamook	5,231	$41,109	330	474	48.1	A
Lincoln City	8,826	$39,344	950	1,179	140.3	B
Depoe Bay	1,805	$57,143	195	222	22.4	B
Newport	10,559	$49,039	959	1,186	135.8	B
Toledo	3,579	$60,455	320	370	46.8	B
Waldport	2,055	$47,971	211	250	29.1	B
Florence	8,921	$42,356	905	1,119	137.3	C
North Bend-Coos Bay	25,881	$50,905	1,653	2,107	240.9	D
Bandon	3,100	$32,226	456	540	61.8	D
Port Orford	954	$27,500	281	337	57.1	D
Gold Beach	22,418	$42,625	284	321	49.2	D
Brookings	6,431	$62,384	856	985	152.6	D
Full Network	**112,203**	**-**	**16,370**	**19,111**	**2643.7**	**-**

Probabilistic Network Component Analyses

Road and Bridge Damage Analysis

Using the hazard layers and transportation network, a probabilistic damage analysis was performed for both bridges and roads. Burns *et al.* (2021) conducted a multi-hazard damage analysis for bridges on the transportation network using, among others,

HAZUS fragility curves. The HAZUS fragility curves for bridges include 28 bridge classifications which, for brevity, are not presented here. Burns *et al.* (2021) concluded that the HAZUS landslide and liquefaction fragility curves tend to overestimate bridge damage. Therefore, only ground shaking from the earthquake and tsunami inundation were considered here. The resulting damage state probabilities were used in this study.

The road damage analysis was conducted using HAZUS roadway fragility curves (FEMA, 2013; FEMA, 2015). Earthquake intensity measure was permanent ground deformation, whereas inundation depth was used for the tsunami. For consistency with the bridge damage analysis of Burns *et al.* (2021), landslides, lateral spreading, or liquefaction was not considered for the road damage analysis.

The bridge damage state probabilities from Burns *et al.* (2021) were directly sampled in a Monte-Carlo simulation, whereas damage to the road segments were simulated according to the approach outlined in Baker (2008) and used by Kameshwar *et al.* (2019) and Sanderson *et al.* (2021) to estimate damage to the transportation network in Seaside, OR. That is, the probability that the damage state, *DS*, of each road segment exceeds damage state *i* was computed as:

$$P(DS \geq ds_i|D) = P(C_i < D) \quad (1)$$

where D is the demand at the road segment, and C_i is the damage capacity associated with damage state ds_i. The damage capacity of each road segment was simulated as a lognormal random variable, $LN(\cdot)$, computed as:

$$C_i \sim LN(\theta_i, \beta_i) \quad (2)$$

where θ_i and β_i are the median and dispersion parameters associated with the damage capacity of damage state ds_i. The parameterizing medians and dispersion values are shown in Tables 2 and 3 for earthquake peak ground deformation (PGD) and tsunami inundation depth, respectively. Although correlation across road segments was not considered here, this could be accounted for by simulating a multivariate lognormal distribution (Yang *et al.*, 2009).

Table 2: Road fragility parameterization from Peak Ground Deformation (PGD).

	Major Road		Urban Road	
Damage State	Median PGD (θ) [m]	Dispersion (β) [m]	Median PGD (θ) [m]	Dispersion (β) [m]
Slight	0.30	0.0178	0.15	0.0178
Moderate	0.61	0.0178	0.30	0.0178
Extensive	1.52	0.0178	0.61	0.0178

Complete	1.52	0.0178	0.61	0.0178

Table 3: Road fragility parameterization from tsunami inundation depth. The median, θ, and dispersion, β, are dependent on the flow speed, u.

	Low Flow ($u \leq 1$ m/s)		Moderate Flow ($1 < u \leq 5$ m/s)		High flow ($u > 5$ m/s)	
Damage State	Median inundation depth (θ) [m]	Dispersion (β) [m]	Median inundation depth (θ) [m]	Dispersion (β) [m]	Median inundation depth (θ) [m]	Dispersion (β) [m]
Slight	0.67	0.12	0.48	0.15	0.42	0.15
Moderate	1.28	0.12	0.91	0.15	0.80	0.15
Extensive	2.07	0.12	1.48	0.15	1.30	0.15
Complete	3.35	0.12	2.39	0.15	2.10	0.15

A total of 1,000 iterations were performed resulting in discrete damage states for each road and bridge and for both hazards. The multi-hazard damage state was then computed using the Boolean logic rules outlined in the HAZUS tsunami methodology manual:

$$DS_{EQ,Tsu} = max(DS_{EQ}, DS_{Tsu}) \quad (3)$$

$$DS_{EQ,Tsu} = Extensive, if: \{DS_{EQ} = moderate \; and \; DS_{Tsu} = moderate\} \quad (4)$$

$$DS_{EQ,Tsu} = Complete, if: \{DS_{EQ} = extensive \; and \; DS_{Tsu} = extensive\} \quad (5)$$

Where DS_{EQ} and DS_{Tsu} are the discrete earthquake and tsunami damage states associated with each Monte-Carlo iteration. For bridges that lie on a road segment, the bridge damage state is assumed rather than the underlying road damage state. If multiple bridges were located on a single road segment, the maximum damage state of the bridges was used.

Restoration and Functionality

The restoration and functionality of roads and bridges were computed using HAZUS restoration curves, which are represented as a normal cumulative distribution function (CDF) and parameterized via a mean and standard deviation. Functionality is

defined as the percentage of the component that is expected to be open or operational (FEMA, 2013). Restoration curves indicate the functionality of road segments and bridges as a function of time and were computed as:

$$f(t) = \Phi\left(\frac{t - \mu_{ds_i}}{\sigma_{ds_i}}\right) \quad (6)$$

where $f(t)$ is the functionality of the road or bridge, t is time in days after the event, μ_{ds_i} and σ_{ds_i} are the mean and standard deviation associated with damage state ds_i, and $\Phi(\cdot)$ denotes the standard normal CDF. The road and bridge restoration curves are shown in Figure 4. The means and standard deviations are shown in Table 4 and vary depending on the infrastructure type (road or bridge), the type of hazard (earthquake ground motion or tsunami inundation), and the degree of damage (slight, moderate, extensive, or complete).

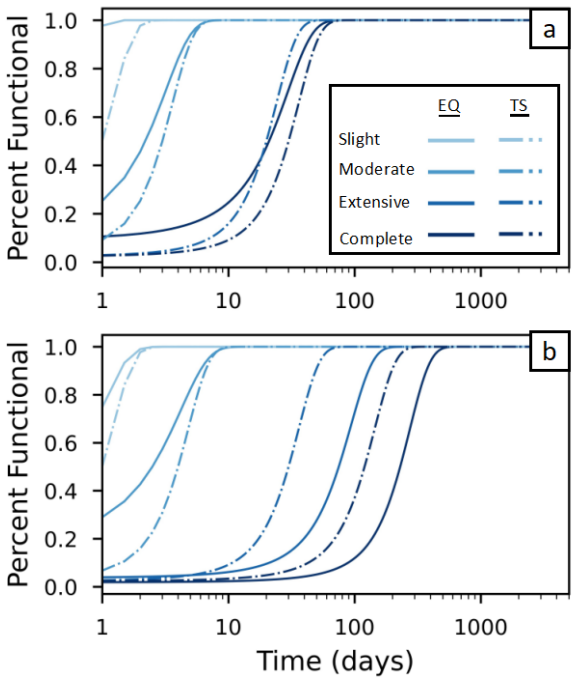

Fig. 4. Restoration curves for earthquake ground shaking (EQ) and tsunami inundation (TS) associated with (a) roads and (b) bridges.

Table 4: Road and bridge restoration curve parameterization.

	Road	Bridge

Damage State	Earthquake Mean [days]	Earthquake Std Dev. [days]	Tsunami Mean [days]	Tsunami Std. Dev. [days]	Earthquake Mean [days]	Earthquake Std. Dev. [days]	Tsunami Mean [days]	Tsunami Std. Dev. [days]
Slight	0.9	0.05	1	0.05	0.6	0.6	1	0.5
Moderate	2.2	1.8	3	1.5	2.5	2.7	4	2
Extensive	21	16	20	10	75	42	30	15
Complete	21	15	30	15	230	110	120	60

To account for limitations in resources, the restoration curves were modified at both the regional and local scales. At the regional scale, restoration was prioritized according to the tiers shown in Figure 2. Each subsequent tier began restoration following all roads and bridges in the prior tier reaching a randomly sampled functionality level. Here, the necessary functionality level to begin restoration of the following tier followed a normal distribution with mean 0.5 and a standard deviation of 0.1. For example, if this value was sampled as 0.6, all Tier 1-Phase 1 roads and bridges must have reached 0.6 functionality following the restoration curves of Figure 4 before any Tier 1-Phase 2 road segments began restoration. The assumption is that not all roads and bridges will begin being repaired immediately due to limitations in resources. Note that in this work, the mean of 0.5 and standard deviation of 0.1 were assumed; however, these values could be refined in future work based on regional preparation levels. That is, if a region has a good preparation level, then the parameterizing mean could be lower, thus indicating that subsequent tiers initiate their restoration process sooner. The resulting average regional functionality across all 1,000 iterations at days 1, 60, 90, and 720 are shown in Figure 5.

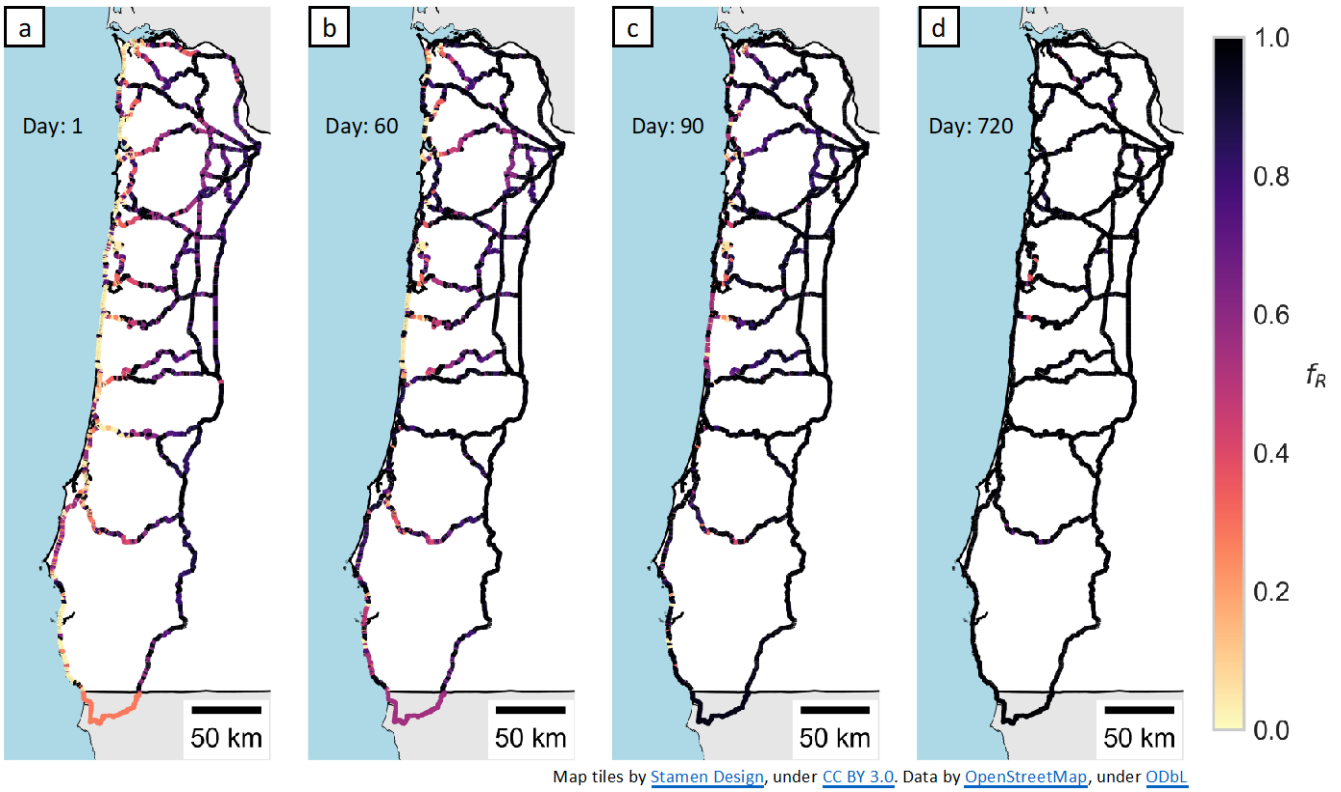

Fig. 5. Restoration of regional road network. Average functionality, f_R, of the regional roads and bridges is shown at (a) Day 1, (b) Day 60, (c) Day 90, and (d) Day 720. $f_R = 0$ is nonfunctional, $f_R = 1$ is fully functional.

At the local scale, the functionality of roads and bridges were modified based on accessibility to the maintenance facilities. It was assumed that communities rely on supplies from the maintenance facilities to repair their roads and that communities located further from their respective maintenance facility will take longer to receive these supplies. The standard functionality was thus modified for local roads as:

$$f_L(t) = f(t) \cdot \delta^k \tag{7}$$

where f was taken from equation (6) and δ was computed as:

$$\delta(t) = \frac{T_{(o,d),0}}{T_{(o,d),t}} \tag{8}$$

where $T_{(o,d),t}$ represents the travel time along the shortest path between origin o and destination d at time t. Here, the origin was taken as the maintenance facility and the destination as the community of interest. The reference time in the numerator is 0, thus indicating pre-disturbance travel times. As the regional network recovers, the post-disturbance travel time in the

denominator approaches the pre-disturbance travel time and δ approaches 1. Values of δ, thus, range between 0 and 1. The constant k in equation (7) was defined as:

$$k = \begin{cases} 0.5; & T_{(o,d),0} < 1hr \\ 1; & 1hr \leq T_{(o,d),0} < 2hrs \\ 2; & T_{(o,d),0} \geq 2hrs \end{cases} \quad (9)$$

With this formulation, the assumption behind k is that more trips can be made between communities closer to their maintenance facility than those located further. The values of k were assumed; however, these could be refined in future work based on models that are dependent on resources available at the origin and destination. For example, if resources for repair are limited and prioritized by community, k can be a time dependent function that approaches 0 as resources are allocated from maintenance facilities to each community. Thus, when $k = 0$, $\delta = 1$, and the local functionality is taken directly from equation (6). The term δ^k introduces a one-way dependence of the local network restoration on the regional network restoration. The average local functionality at Newport across all 1,000 iterations at days 1, 60, 90, and 720 are shown in Figure 6.

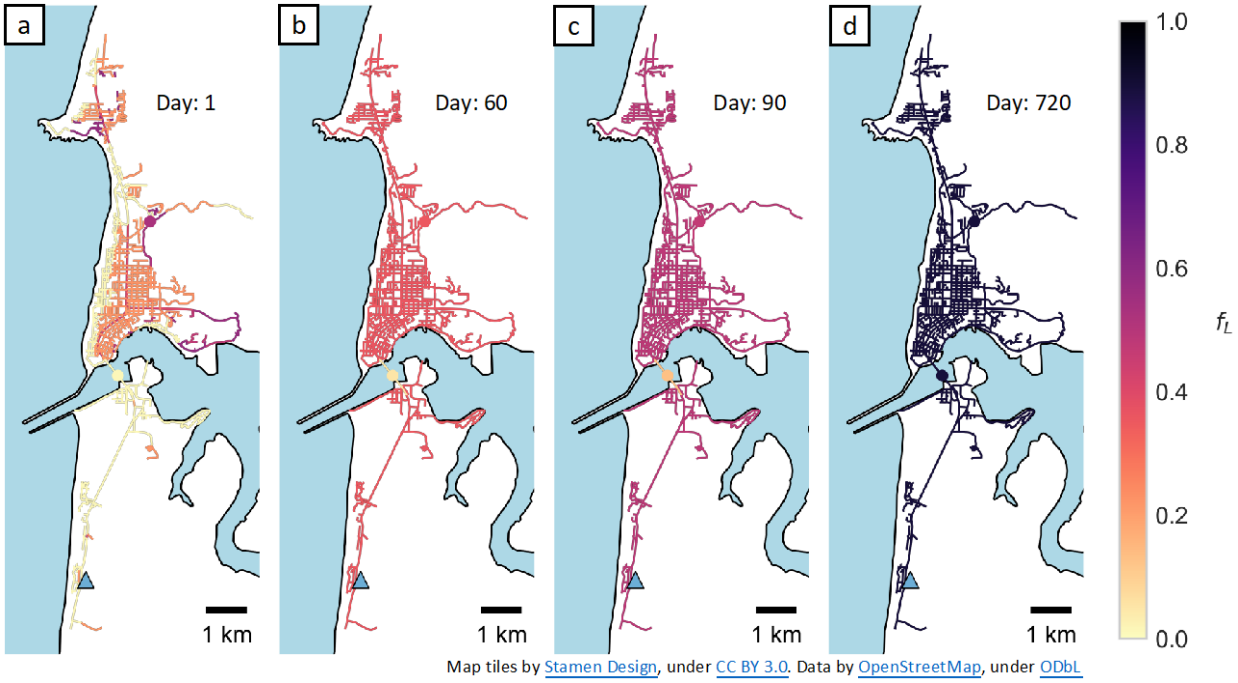

Fig. 6. Restoration of local road network for Newport. The average functionality of local roads and bridges at (a) Day 1, (b) Day 60, (c) Day 90, and (d) Day 720. $f_L = 0$ is nonfunctional, $f_L = 1$ is fully functional.

Functionality-Based Travel Time Surface

The local and regional functionality of roads and bridges were then related to increased travel times along these segments. A commonly used relationship between travel times, traffic capacities, and traffic volumes is the Bureau of Public Roads (BPR) curve (Martin and McGuckin, 1998), computed as:

$$T'_{c,s} = T'_{o,s}\left(1 + \alpha\left(\frac{v_s}{c_s}\right)^{\beta}\right) \tag{10}$$

where $T'_{c,s}$ and $T'_{o,s}$ are the current and original travel times along segment s, α and β are constants typically taken as 0.15 and 4, respectively, under normal flow conditions, and v_s and c_s are traffic volume and capacity, respectively, along segment s.

It was assumed that immediately after the rupture of the CSZ, the traffic volume on the regional road network will initially be limited and gradually return to pre-disturbance conditions. The traffic volume, v_s, was modified by a traffic volume multiplier, $\varphi(t)$, which was defined as a normal CDF with a mean of 30 days and a standard deviation of 14 days. The traffic volume multiplier is similar to the restoration curves of Figure 4, in that a normal CDF is used to define a unitless curve that is a function time following the disaster. The traffic volume multiplier is simply used to reduce the traffic volume along road segment s. The parameterizing mean and standard deviation were assumed for this work and can be refined in future work based on output from post-disaster traffic forecasting models. The BPR curve in equation (10) was thus modified to account for reductions in traffic volume and regional road and bridge functionality, f_R, as:

$$T'_{c,s} = T'_{o,s}\left(\frac{1}{f_R} + \alpha\left(\frac{\varphi \cdot v_s}{f_R \cdot c_s}\right)^{\beta}\right) \tag{11}$$

A normalized version of equation (11) is shown in Figure 7 as a function of $\frac{\varphi \cdot v_s}{c_s}$ and f_R. Each contour corresponds to values of $T'_{c,s}/T'_{o,s}$. Along the top axis, where $f_R = 1$, the standard BPR curve of equation (10) is obtained. Along the leftmost axis where $v \cdot \varphi = 0$, *i.e.,* there is no traffic volume, the travel time is increased by $T'_{o,s}/f_R$. For example, a road or bridge that is 50% functional results in double the travel time. This formulation accounts for a reduction in both traffic volume and road and bridge capacity. Alternative formulations to compute post-disaster traffic volumes and travel times exist such as gravity models and user-equilibrium traffic assignment (Shiraki *et al.,* 2007; Guo *et al.,* 2017); however, these were not implemented here as they require origin-destination trip assignments. The travel time surface was employed where traffic volume data is available, *i.e.,* on the regional network. On the local networks, the travel time along a road segment was increased by $T'_{c,s} = T'_{o,s}/f_L$.

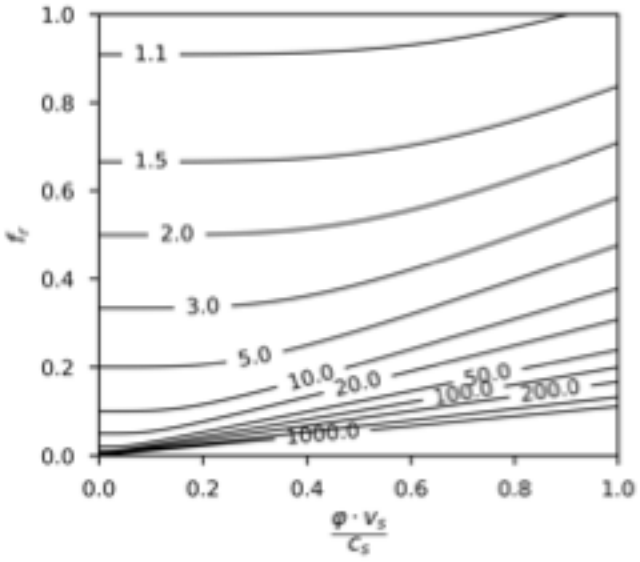

Fig. 7. Travel time surface used to relate traffic volume, traffic capacity, and functionality of roads and bridges. Each contour corresponds to values of $T'_{c,s}/T'_{o,s}$.

Results of Application to a Transportation Network

Whereas the previous section followed steps 1 and 2 of the generalized framework shown in Figure 1, this section follows step 3. That is, the network is considered as a system, and both regional and local metrics are defined to evaluate the resilience of the transportation network at multiple spatial scales. Further, it is demonstrated how this framework can be used as decision support tool.

Regional Connectivity Index

The assumed role of the transportation network was to provide post-disaster aid to communities, and the location of airports were used as a proxy for supply sources. Airports take on the role of service origin and were grouped into 3 tiers as shown in Figure 2. To define accessibility from these supply sources to the coastal communities, or service destinations, a regional connectivity index, *RCI*, was created. The *RCI* is based on the concept of travel time resilience (Omer, 2011), and was defined as:

$$RCI(t) = \sum_{j \epsilon Tiers} w_j \frac{\min_{o \epsilon Tier j} T_{(o,d),0}}{\min_{o \epsilon Tier j} T_{(o,d),t}} \quad (12)$$

where $T_{(o,d),t}$ is the travel time along the shortest path between origin o and destination d at time t. At each time step t, the transportation network was updated according to the methodology outlined in the previous section, and the shortest path recomputed using this updated network. The python package NetworkX was used for computing the shortest path between nodes (Hagberg *et al.*, 2008). Airports were taken as the origins whereas the communities were taken as the destinations. The time in the numerator is $t = 0$, thus indicating pre-disturbance travel times. Each airport tier was represented by the variable j, *e.g.*, j=1, 2, and 3. The variable w_j is a weight that represents the importance of airport tiers, and the summation of weights across all tiers is equal to one. The weights were included to prioritize airport tiers depending on interests and features such as runway capacity and local logistics. By formulating the *RCI* as such, each community's index was normalized by their respective travel time under normal circumstances, *e.g.*, pre-disturbance travel times. This metric thus helps identify which communities were furthest displaced from their pre-disturbance conditions. By tracking the *RCI* across time and considering the network recovery, each trajectory will re-approach 1, where the post-disturbance travel times are identical to the pre-disturbance travel times.

Figure 8 shows the *RCI* for Cannon Beach, Newport, and Port Orford for all 1,000 iterations and with equal weights across all three airport tiers. These three communities are in the north, central, and south coast respectively. The solid blue line indicates the average of all iterations at each time step, whereas the shaded region shows plus/minus one standard deviation. Figure 8c shows that on average, the *RCI* of Port Orford begins at approximately 0.18, thus indicating that across all airport tiers it takes about 5 times as long as the pre-disturbance travel time to access the community. The recovery trajectory shows that on average, the accessibility to Port Orford is fully re-established around 2.4 years after the CSZ. Conversely, the *RCI* of Cannon Beach begins on average at approximately 0.5, indicating that across all tiers the travel time to these airports is about doubled. Figure 8 shows that on average Cannon Beach recovers approximately 1.75 years after the event. The low initial *RCI* and slower recovery time of Port Orford is due to its location within the larger regional network. The nearest Tier 1 and 3 airports are both located along Interstate 5 with no direct route to Port Orford, *e.g.*, the shortest path is from either the south through California or north through Bandon.

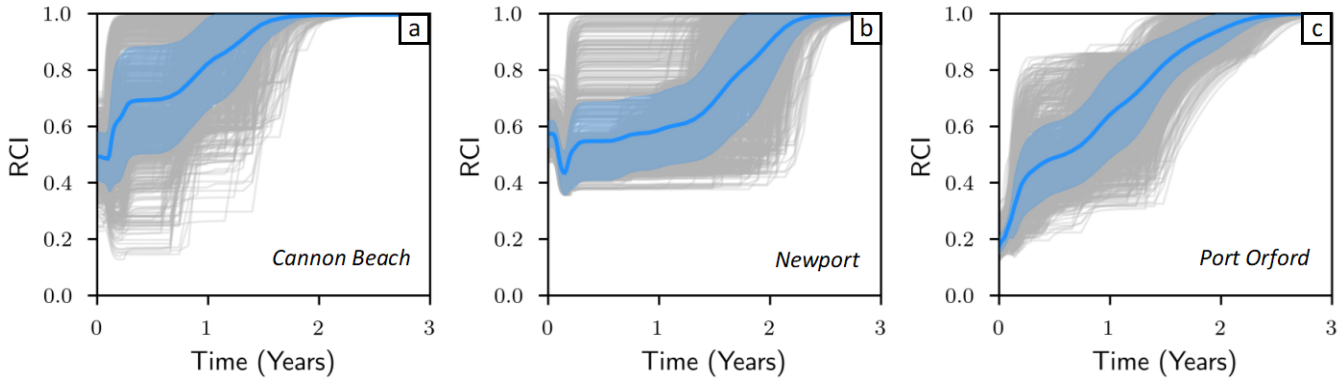

Fig. 8. Regional Connectivity Index (RCI) for (a) Cannon Beach, (b) Newport, and (c) Port Orford. The grey lines correspond to each iteration of the Monte-Carlo simulation, the thick blue line is the average curve, and the shaded region indicates the plus/minus one standard deviation range.

Perhaps counterintuitively, Figure 8 shows that some of the *RCI* trajectories see a slight reduction before monotonically recovering. This occurs during all iterations for Newport and a handful of iterations for Cannon Beach. This is due to the form of the travel time surface and tradeoffs between road restoration and increased traffic volumes as a function of time. Port Orford does not see these reductions in *RCI* as it is located along the south coast and the southern highways are prioritized later for restoration, *e.g.,* after the traffic volumes are restored to pre-disturbance conditions.

Uncertainty in the *RCI* trajectories of Figure 8 stem from both uncertainty in the initial road/bridge damage states and the tiered restoration process of the regional network. Further, correlations across road segment damage states was not considered here which contributes to the overall uncertainty when considering the network as a whole.

Local Connectivity Index

At the local scale, a local connectivity index, *LCI*, was introduced to measure the overall local network resilience. Similarly based on the concept of travel time resilience, the *LCI* was defined as:

$$LCI(t) = \left(\sum_{o \in S}\sum_{d \in S} T_{(o,d),0}\right) \Big/ \left(\sum_{o \in S}\sum_{d \in S} T_{(o,d),t}\right) \tag{13}$$

where $T_{(o,d),t}$ is the travel time along the shortest path between origin o and destination d at time t. Nodes o and d are taken from a subsample of nodes, S, of the entire local network. The nodes that comprise S were randomly sampled during each iteration from the local network. A reduction factor was introduced that scales down the number of nodes within each local network, here taken as 32. So, for example, if a local network had 1,280 nodes, a reduction factor of 32 resulted in the subsample being comprised of 40 nodes. The shortest path between all possible combinations of these 40 nodes was computed. This reduced the number of origin-destination pairs from 818,560 to 780. Sensitivity testing, although not shown here, indicated that across all iterations the use of the reduction factor of 32 provided an accurate estimate of the mean *LCI* while significantly reducing computational costs. Use of the reduction factor did, however, result in increased uncertainty.

The results of this *LCI* formulation for Cannon Beach, Newport, and Port Orford are shown in Figure 9. The dash-dot line indicates the mean *LCI* if damage to the regional network is not considered. For these three communities, the *LCI* starts near 0 and recovers at different rates. The low initial *LCI* is driven by the network damage sustained by coastal communities as these

are closer to the CSZ and hazard intensity measures are larger. The results for Newport show similar reductions in *LCI* as that of the *RCI* from Figure 8. This is due to the one-way dependence of the local network on the regional network and accessibility to maintenance facilities. Similarly, Port Orford has a slow time to recover due the one-way dependence.

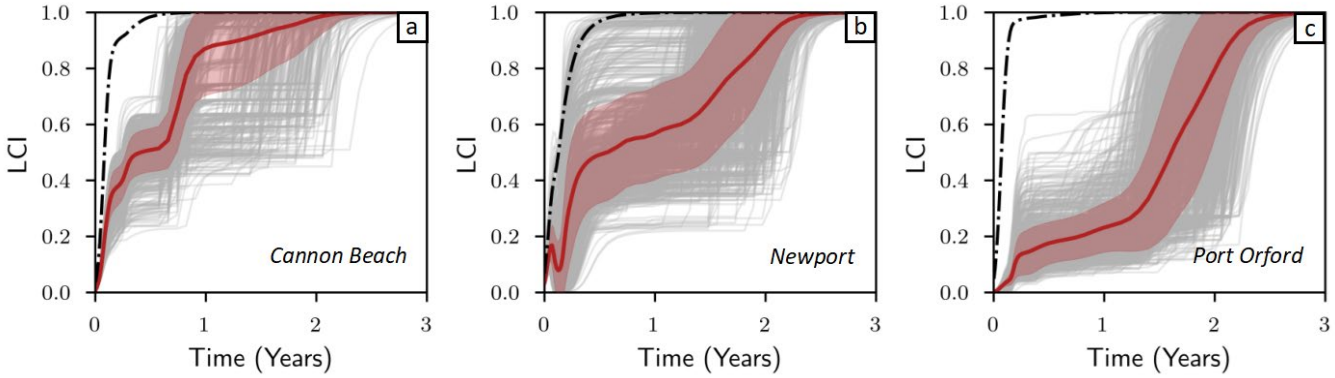

Fig. 9. Local Connectivity Index (LCI) for (a) Cannon Beach, (b) Newport, and (c) Port Orford. The grey lines correspond to each iteration of the Monte-Carlo simulation, the thick red line is the average, and the shaded region indicates the plus/minus one standard deviation range. The dash-dot black line indicates the mean LCI when the regional network is not considered.

Similar to Figure 8, uncertainty in the *LCI* trajectories of Figure 9 are due to the initial road/bridge damage states, no correlation across damage states, and the tiered restoration process of the regional network. Another source of uncertainty in the *LCI* is that a subsample of origin-destination nodes are employed, rather than the entire network.

Considering both regional and local resilience

Having established both the *RCI* and *LCI*, the status of the network at multiple scales was evaluated. Figure 10 shows the mean *LCI* and *RCI* at each time step plotted against each other for six of the eighteen communities. The results for the mean *LCI* and *RCI* for the three communities discussed in detail previously, Cannon Beach, Newport, Port Orford, are shown in 10a-c. Three more communities, Rockaway Beach, Lincoln City, and Toledo are shown in 10d-f to demonstrate differences in recovery trajectories. Both the *RCI* and *LCI* range between 0 and 1. Each marker corresponds to days 1, 30, 60, 180, 360, and 720. Four quadrants are identified in Figure 10. A trajectory that passes through the lower right quadrant indicates that the local recovery outpaces the regional recovery and thus a community may have reestablished their local network but remains isolated from the rest of the region. Conversely, a trajectory that passes through the upper left quadrant conveys the opposite. That is, the community is accessible from the rest of the region, but the local network has not been reestablished to the same level of functionality.

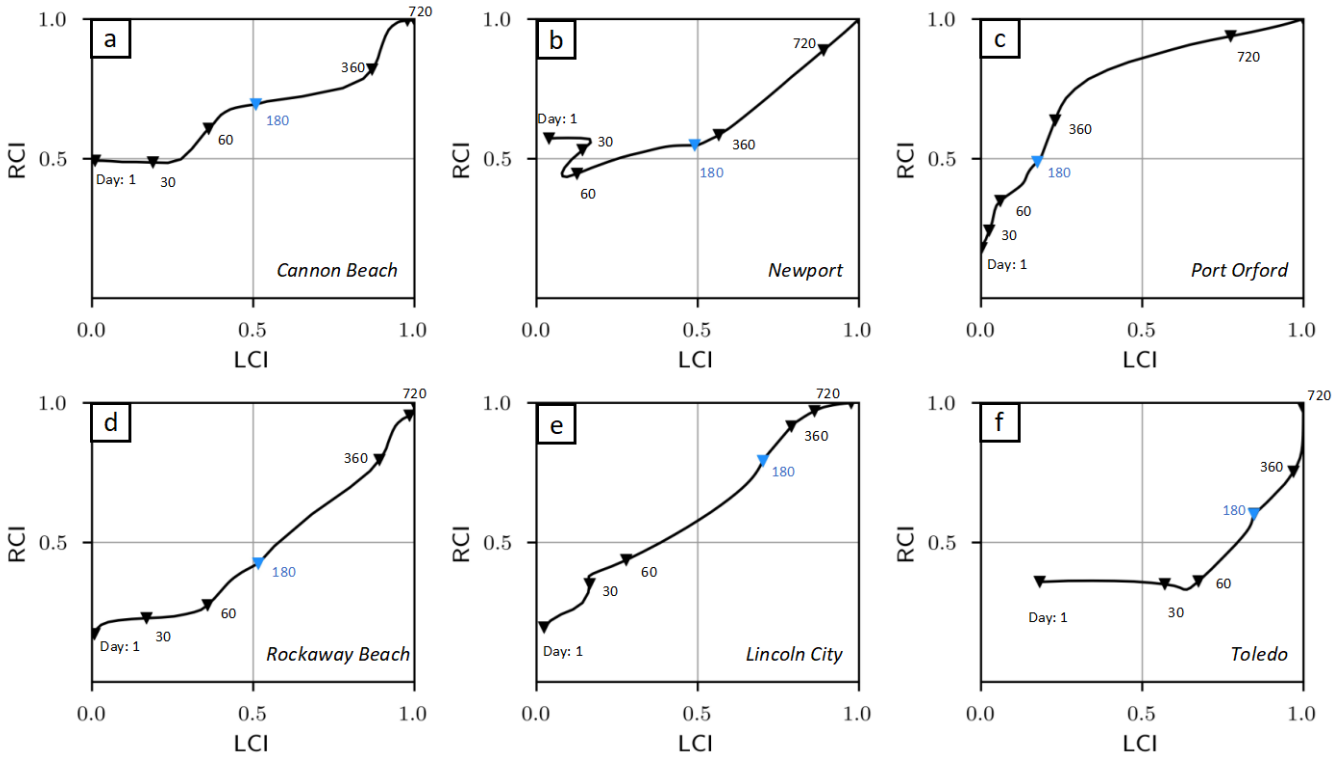

Fig. 10. RCI vs. LCI recovery trajectories for (a) Cannon Beach, (b) Newport, (c) Port Orford, (d) Rockaway Beach, (e) Lincoln City, and (f) Toledo.

Of the communities shown in Figure 10, Port Orford (10c) has a regional recovery that initially outpaces the local recovery, thus indicating that aid from the airports may be able to reach the community, however the local network is still not repaired to the same level of functionality. Conversely, Toledo shown in panel 10f, exhibits the opposite trend. That is, the local recovery outpaces the regional recovery, indicating that the local network is recovering quicker; however, the community has poor access to the airports throughout the region.

Both Cannon Beach (10a) and Newport (10b) show a robust initial *RCI* compared to the *LCI*. For both communities, the regional recovery is initially slow while the local network is being repaired. The dips in the *RCI* and *LCI* that were previously identified for Newport are shown in Newport's trajectory, as both the *RCI* and *LCI* decrease around day 30 before beginning a monotonic recovery.

Rockaway Beach (10d) and Lincoln City (10e) show recovery trajectories that are both near to a 45-degree line, indicating that the regional and local connectivity indices are on pace with each other. While these trajectories appear nearly identical, the temporal component to these plots should be considered. Whereas Lincoln City is approaching a full recovery around day 180, Rockway Beach is only halfway recovered.

The recovery trajectories of the six communities shown in Figure 10 emphasize how communities recover not in isolation from the rest of the region, but in concert with the regional network. Aside from Toledo (10f), the local recovery of the communities shown in Figure 10 are highly dependent on the recovery of the regional network. That is, the regional recovery either outpaces or is in line with the local recovery. This further emphasizes the need for local networks to be considered in a larger network following regional disasters.

The *RCI* and *LCI* can further be used to determine the time until a community returns to some index threshold at both the regional and local scales. Figure 11 shows, for all 18 communities, the time until: (a) the *RCI* exceeds 0.75, (b) the *LCI* exceeds 0.75, and (c) both the *RCI* and *LCI* exceed 0.75. The selection of the value of 0.75 is subjective and was selected as this corresponds to travel times that are 1.33 times longer than pre-disturbance conditions and are thus approaching "near-normal". While not shown here, a sensitivity analysis indicates that regardless of whether 0.7, 0.75, 0.8, or 0.9 are chosen as an exceedance threshold for the *LCI/RCI*, the relative comparisons across communities remain similar. The figure is oriented such that each community is shown from north (Astoria-Warrenton) to south (Brookings). Uncertainty is quantified via violin plots, which are nonparametric distributions of all 1,000 iterations. The mean time until exceedance is shown via the markers.

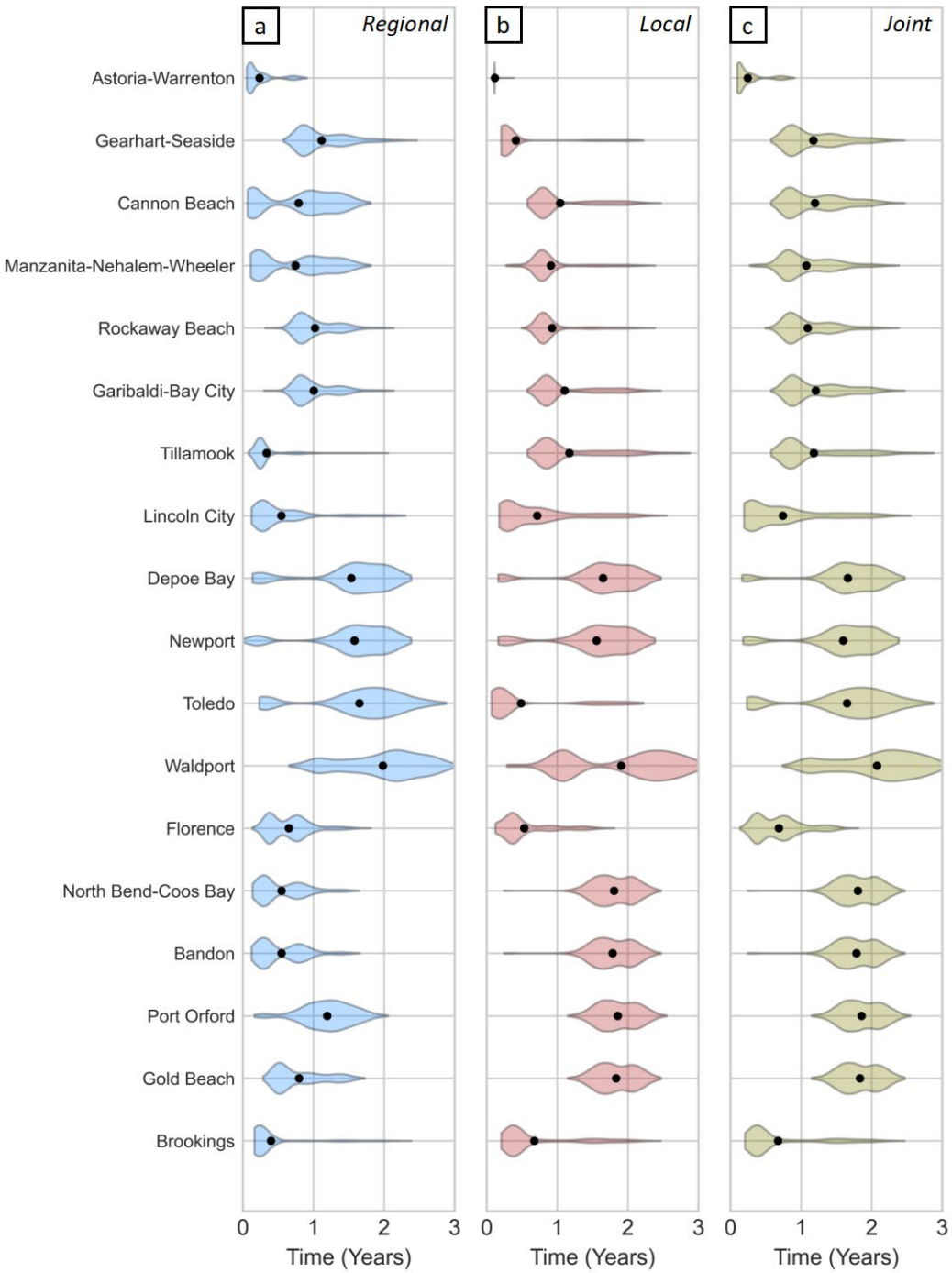

373

374 **Fig. 11**. Time in years required for the connectivity index to exceed 0.75 for the (a) RCI, (b) LCI and (c) joint RCI and LCI.
375 Dots indicate the mean time to exceed 0.75.

376 Considering the time until the *RCI* exceeds 0.75 in Figure 11a, notable trends between the location of a community within the
377 regional network and the time to recover can be obtained. The faster recovering communities are either (1) located along a Tier

1-phase 2 road, *e.g.*, Astoria-Warrenton, Tillamook, Lincoln City, Florence, and North Bend-Coos Bay, or (2) the connecting roads to the rest of the region are not located along the coast, *e.g.*, Bandon and Brookings. A handful of these communities share both features. For example, Astoria-Warrenton is located at the tail of a Tier 1-phase 2 road that does not run directly along the coast and, subsequently, results in the fastest regional recovery. It is interesting to note that although a community may be located on a Tier 1-phase 2 road, this does not necessarily guarantee a fast recovery, *e.g.,* Newport. This is due to the connecting roads being located along the coast and thus subject to larger hazard intensity measures.

Figure 11c shows that Astoria-Warrenton has the quickest average joint time to recover followed by Florence, Brookings, and Lincoln City. The fast recovery of Astoria-Warrenton is driven by the regional recovery, and at the local scale by the maintenance facility located within the urban growth boundary. Because there is a maintenance facility located within the urban growth boundary, the local restoration follows the HAZUS restoration curves exactly.

Similar to Astoria-Warrenton, Florence is located at the tail of a Tier 1-Phase 2 road and exhibits a fast recovery. Compared to the neighboring communities, Waldport and North Bend-Coos Bay, the recovery of Florence is significantly faster. This is driven by a couple of factors. On one hand, Waldport is only accessible via Tier 3 and undefined roads, thus the regional recovery is slow. This is apparent in Figure 11a, as the mean regional time to recover for Waldport is approximately 2 years compared to less than a year for Florence. South of Florence, North Bend-Coos Bay is also situated on a Tier 1-Phase 2 road and can be seen to have a similar regional recovery time. However, the local recovery of North Bend-Coos Bay is nearly a year longer than that of Florence. This variation in local recovery between the two communities is due to Florence and North Bend-Coos Bay being in different maintenance facility districts (Table 1 and Figure 2). In this case, Florence has better accessibility to the assigned maintenance facility *C*, compared to that of North Bend-Coos Bay which is assigned maintenance facility *D*.

The community of Brookings has a quick average recovery time because of the Tier 2 airport located within the urban growth boundaries, and the community is not subject to liquefaction. Because of the latter, only the tsunami hazard impacts the performance of the local road network.

Each of the coastal communities can be delimited as north-coast (Astoria-Warrenton to Tillamook), central-coast (Lincoln City to Florence), and south-coast (North Bend-Coos Bay to Brookings). Considering these groupings, trends in time to recover can be identified. For example, amongst the north-coast communities, Gearhart-Seaside to Tillamook have similar recovery times whereas Astoria-Warrenton recovers nearly a year before. For the central-coast, both Lincoln City and Florence recover faster than the other four communities. And for the south-coast, Brookings recovers faster. The fast recovery time of these four communities within their respective north-, central-, south-coast distinctions could indicate that these communities be used as coastal hubs for post-disaster restoration efforts.

Decision Support

Two variations in how this framework can be used as a decision support tool are shown in Figure 12. Figure 12a shows how the weighting parameter of equation (12) impacts the mean time to the restore the *RCI* to 0.75. The points corresponding to 'All Tiers' are the same as the mean values from Figure 11a in which all airport tiers were weighted equally. The points labeled 'Any Tier' correspond to the minimum time for the *RCI* to exceed 0.75 considering each airport tier individually. Interestingly, north coast communities see little to no variation when considering each airport tier individually. Conversely, the central and south coast communities do see deviations, indicating that they may be accessible to certain airports but not to all. Tier 2 and 3 airports are located along the coast in some central and south coast communities. Thus, if these airports can accommodate post-disaster needs, the south coast communities may recovery just as fast, if not faster, than the north coast communities.

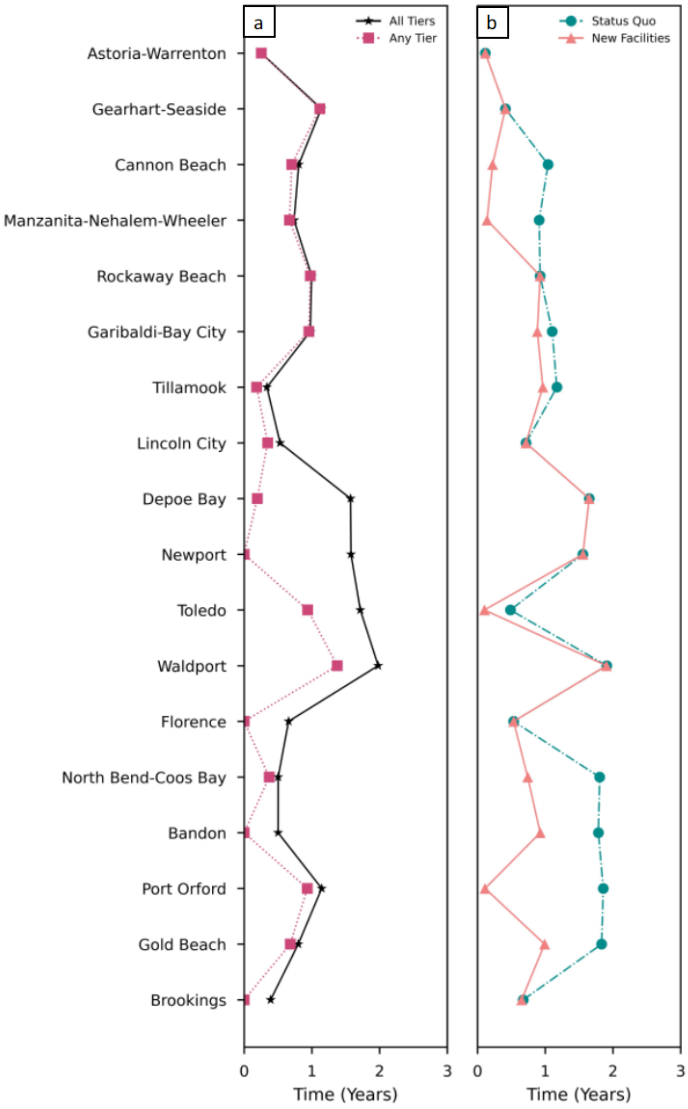

Fig. 12. Example of using framework as a decision support tool: (a) time for the RCI to exceed 0.75 considering different airport tier weightings, and (b) time for the LCI to exceed 0.75 under both status quo conditions and with additional maintenance facilities

Figure 12b shows the effect that adding additional maintenance facilities has on the time to restore the *LCI* to 0.75. This further highlights dependencies between the regional and local networks in that the maintenance facilities located throughout the region have an impact on local network restoration. In addition to the four maintenance facilities shown in Figure 2, three additional facilities were added to the network in the communities of Wheeler, Toledo, and Port Orford. Figure 12b shows the mean time until the *LCI* exceeds 0.75 for both the status quo conditions, *e.g.,* the same points shown in Figure 11b, and with the addition of three new maintenance facilities. The beneficial effect that a new maintenance facility in Port Orford has on the south coast communities is apparent as these communities see a reduction in the time until the *LCI* exceeds 0.75. North coast communities, Manzanita-Nehalem-Wheeler, and Cannon Beach see improvements with the addition of a maintenance facility in Wheeler. The remaining communities do not see as much of an improvement either because they already have a short time to recover, or their assigned maintenance facility is the same as the status quo conditions.

Discussion

The methodology that was developed can be used to aid discussions in mitigation planning along multiple fronts. First, due to increases in travel time that may result from natural hazards, individuals residing in communities may face a sense of "islanding" or isolation from the rest of the region or their local community. For example, if the travel time between two communities begins to increase beyond expectations, *e.g.,* what used to be a one-hour trip now takes five-hours, individuals may feel isolated from the rest of the region. Planning guides have alluded to this concept without explicitly defining what constitutes an "island" (CH2M Hill, 2012; CREW, 2013; OSSPAC, 2013). The *RCI* and *LCI* could serve as means to quantify this. For example, decision makers may identify that if a community is below a threshold of 0.2, *e.g.,* a five-times increase in travel time relative to pre-disturbance conditions, then this establishes an island. Further, rather than a connectivity index, an islanding index could be formulated, *e.g.*, one minus the *RCI* or *LCI*, to define the severity of islanding.

In addition, results from this methodology emphasize the necessity of considering post-disaster performance and restoration of local networks within a larger regional setting. Use of restoration curves without consideration given to regional-level restoration efforts may lead to underpredicting the time to recover. It was shown that by applying HAZUS restoration curves without regional considerations, the *LCI* will approach 90% recovery within a couple of months. With regional considerations, the framework presented here estimates a recovery times well beyond 1-year for most coastal communities. Future research could aim to refine the post-disaster dependencies and interdependencies of local networks within larger regional settings.

Some assumptions to implement the methodology were made. First, no damage to airports were considered, and it was assumed that temporary measures were employed to quickly resume operations. This has been observed for air traffic control towers in prior earthquakes (e.g., Almufti *et al.*, 2014). Damage to airports could however be considered in future work by using airport fragility curves and restoration functions similar to those used for roads and bridges. Further, assumptions in the restoration process were made. To account for limitations in resources at the regional scale, the restoration curves were modified by assuming that the restoration of higher priority tiers needed to reach a randomly sampled functionality level. Alternative approaches for quantifying the restoration of infrastructure systems exist and could be employed in future work (Costa *et al.*, 2021; Wang and van de Lindt, 2021). Further, the traffic volumes on the road network were assumed to be zero immediately after the event and slowly recover to pre-disturbance conditions. Alternative approaches to account for post-disaster traffic volumes exist and could also be incorporated (Dong *et al.,* 2016; Guo *et al.,* 2017). Minor assumptions include both the location of maintenance facilities and the grouping of nearby communities into one large community, *e.g.,* Astoria-Warrenton and Gearhart-Seaside.

Despite these assumptions, the framework can still aid stakeholders in mitigation planning. As the recovery of infrastructure systems following disasters involve multiple actors that do not follow physical laws, there is large uncertainty and complexity regarding both accurate and precise estimates of the time it takes to recover. As such, this framework is not intended to be predictive in the sense that other models of physical processes may be. Rather, the framework is intended to be used to make comparisons of local versus regional resilience of a given community, *e.g.*, community *A* is more regionally resilient than it is locally resilient, and comparisons across communities, *e.g.*, community *A* is more regionally/locally resilient than community *B*.

In addition to addressing the limitations, future work could also include considering a larger transportation network that extends both further east and into neighboring states. A multi-state network may aid in a more concerted efforted to reduce the impacts of large-scale events. Additionally, critical facilities such as fire stations and hospitals are employed in disaster research and, while important, overlook what community members may value. Thus, this work has the potential to be expanded beyond an engineering perspective to a larger interdisciplinary perspective. Similar to how previous work has considered equitable access to various services via transportation networks (Logan and Guikema, 2020), interview data of what community members value could be transcribed to geospatial locations and employed within this methodology to determine how accessible these locations are for members of a community.

Conclusions

This paper presented a multi-scale framework for simultaneously assessing the regional and local resilience of infrastructure networks following disruptions from natural hazards. The framework is intended to be expandable across different types of

infrastructure networks. A methodology was developed from the generalized framework to demonstrate how it can be applied to a road and highway transportation network under disruption from a multi-hazard Cascadia Subduction Zone earthquake ground shaking and tsunami inundation scenario. By using airports as proxies for the location of supply sources, the application of this methodology provides insights into the resilience of the transportation network at multiple spatial scales. Considering the problem under a multi-scale lens results in both regional and local metrics related to increases in travel times. The regional metric of a community, the *RCI*, considered accessibility from the community boundaries to airports, whereas the local metric, the *LCI*, considered accessibility within the urban growth boundary of the community itself. Comparing the two metrics together provides insights as to how a community fares immediately after an event and during the recovery process at both spatial scales.

By developing a methodology for a transportation network from the generalized framework, several conclusions can be obtained:

1. The post-disaster performance and recovery of local networks should be considered in the context of a larger regional network: The methodology incorporated a one-way dependence of the restoration of local networks on access to resources within the regional network. By comparing the results in this paper to previous work in which regional networks were not considered, the time to recover for a single community was shown to be four-times longer than previously estimated. Further, the recovery of local networks was shown to vary across communities, indicating that communities are sensitive to where they are situated within the regional network.
2. Attributes that lead to regional and local resilience differ: It was shown that regionally resilient communities are not guaranteed to be locally resilient and vice-versa. Communities with a fast regional recovery had access to roads that were both identified as higher priority for restoration and located in areas that are subject to smaller hazard intensity measures. Communities with a fast local recovery were shown to be highly dependent on access to maintenance facilities. In addition, select communities were shown to have attributes that led to a faster recovery relative to neighboring communities and could potentially serve as hubs for restoration efforts.
3. Implementation of mitigation options should be strategically considered and do not guarantee an improvement in the time it takes to recover: It was shown that adding additional maintenance facilities impacted some communities while others saw little to no improvements. In this work, communities that are more rural saw improvements in time to recover when an additional maintenance facility was added in the region. Conversely, communities closer to metropolitan areas saw minimal improvement.

Data Availability Statement

All data, models, or code that support the findings of this study are available from the corresponding author upon reasonable request.

Acknowledgements

We acknowledge funding that supported this research in part from Oregon Sea Grant under award no. NA18OAR170072 (CDFA no. 11.417) from NOAA's National Sea Grant College Program, US Department of Commerce, and by appropriations made by the Oregon State Legislature. We further acknowledge funding as part of the cooperative agreement 70NANB15H044 between the National Institute of Standards and Technology (NIST) and Colorado State University through a subaward to Oregon State University. The content expressed in this paper are the views of the authors and do not necessarily represent the opinions or views of NIST or the U.S Department of Commerce.

References

Almufti, I., Barbosa, A., Bray, J., Dawson, T., Marrow, J., Mieler, M., Scawthorn, C., and Yashinsky, M.. 2014. "M 6.0 South Napa Earthquake of August 24, 2014". *EERI Special Earthquake Report*, *October 2014*. Earthquake Engineering Research Institute (EERI), Oakland, California.

Baker, J. 2008. "Introducing correlation among fragility functions for multiple components". *The 14th World Conference on Earthquake Engineering*, pp. 12-17. Beijing, China.

Buldyrev, S., Parshani, R., Paul, G., Stanley, E., and Havlin, S. 2010. Catastrophic cascade of failures in interdependent networks. *Nature,* 464, 1025-1028. https://doi.org/10.1038/nature08932

Burns, P., Barbosa, A., Olsen, M., and Wang, H. 2021. "Multi-Hazard Damage and Loss Assessment of Bridges in a Highway Network Subject to Earthquake and Tsunami Hazards". *Nat Haz Rev*, 22(2): 05021002. https://doi.org/10.1061/(ASCE)NH.1527-6996.0000429

Cascadia Region Earthquake Working Group (CREW). 2013. "Cascadia Subduction Zone Earthquakes: A Magnitude 9.0 Earthquake Scenario". DOGAMI Open File Report O-13-22.

Cavalieri, F., Franchin, P., and Pinto, P. 2014. "Fragility Functions of Electric Power Stations". *SYNER-G: Typology definition and fragility functions for physical elements at seismic risk,* 157-185. https://doi.org/10.1007/978-94-007-7872-6

Chang, S., and Nojima, N. 2001. "Measuring post-disaster transportation system performance: the 1995 Kobe earthquake in comparative perspective". *Transp Res Part A Policy Pract,* 35, 475-494. https://doi.org/10.1016/S0965-8564(00)00003-3

CH2M Hill. 2012. "Seismic Lifelines Evaluation, Vulnerability Synthesis, and Identification". Prepared for Oregon Department of Transportation. CH2M Hill, Corvallis, Oregon

Costa, R., Haukaas, T., and Chang, S. 2021. "Agent-based model for post-earthquake housing recovery". *Earthq Spectra*, 37(1), 46-72. https://doi.org/10.1177/8755293020944175

Coveney, J., and O'Dwyer, L. 2009. "Effects of mobility and location on food access". *Health Place,* 15, 45-55. https://doi.org/10.1016/j.healthplace.2008.01.010

Crucitti, P., Latora, V., and Marchiori, M. 2004. "Model for cascading failures in complex networks". *Phys Rev*, 69. https://doi.org/10.1103/PhysRevE.69.045104

Dong, S., Mostafizi, A., Wang, H., and Bosa, P. 2016. "Post-Disaster Mobility in Disrupted Transportation Network: Case Study of Portland, Oregon". Proceedings of *the International Collaboration in Lifeline Earthquake Engineering 2016*, 501-507. https://doi.org/10.1061/9780784480342.068. Shanghai, China.

Dong, S., Mostafizi, A., Wang, H., Gao, J., and Li, X. 2020. "Measuring the Topological Robustness of Transportation Networks to Disaster-Induced Failures: A Percolation Approach". *J. Infrastruct Syst,* 26(2): 04020009. https://doi.org/10.1061/(ASCE)IS.1943-555X.0000533

Faturechi, R., and Miller-Hooks, E. 2015. "Measuring the Performance of Transportation Infrastructure Systems in Disasters: A Comprehensive Review". *J. Infrastruct Syst,* 21(1): 04014025. https://doi.org/10.1061/(ASCE)IS.1943-555X.0000212

Federal Emergency Management Agency) (FEMA). 2015. Hazus – MH 2.1 Technical Manual, Multi-hazard Loss Estimation Methodology, Earthquake Manual. Washington, D.C.

Federal Emergency Management Agency (FEMA). 2013. Tsunami methodology technical manual. Washington, D.C.

Gidaris, I., Padgett, J., Barbosa, A., Chen, S., Cox, D., Webb, B., and Cerato, A. 2017. "Multiple-Hazard Fragility and Restoration Models of Highway Bridges for Regional Risk and Resilience Assessment in the United States: State-of-the-Art Review". *J. Struct Eng,* 143(3): 04016188. https://doi.org/10.1061/(ASCE)ST.1943-541X.0001672

Goldfinger, C., Nelson, H., Morey, A., Johnson, J., Patton, J., Karabanov, E., Gutiérrez-Pastor, J., Eriksson, A., Gràcia, E., Dunhill, G., Enkin, R., Dallimore, A., and Vallier, T. 2012. "Turbidite Event History – Methods and Implications for Holocene Paleoseismicity of the Cascadia Subduction Zone". *US Geological Survey Professional Paper* 1661-F. 170p. https://pubs.er.usgs.gov/publication/pp1661F

Gonzàlez, F., Geist, E., Jaffe, B., Kânoglu, U., Mofjeld, H., Synolakis, C., Titov, V., Arcas, D., Bellomo, D., Carlton, D., Horning, T., Johnson, J., Newman, J., Parsons, T., Peters, R., Peterson, C., Priest, G., Venturato, A., Weber, J., Wong, F., and Yalciner, A. 2009. "Probabilistic tsunami hazard assessment at Seaside, Oregon, for near- and far-field seismic sources. *J. Geophys. Res*. 114. https://doi.org/10.1029/2008JC005132

Guo, A., Liu, Z., Li, S., and Li, H. 2017. "Seismic performance assessment of highway bridge networks considering post-disaster traffic demand of a transportation system in emergency conditions". *Struct Infrastruct Eng,* 13(12), 1523-1537. https://doi.org/10.1080/15732479.2017.1299770

Hagberg, A., Schult, D., and Swart, P. 2008. "Exploring network structure, dynamics, and function using NetworkX". In *Proc., 7th Python in Science Conference,* edited by G. Varoquaux, T. Vaught, and J. Millman, 11-15. Pasadena, CA.

Horner, M., and Widener, M. 2011. "The effects of transportation network failure on people's accessibility to hurricane disaster relief goods: a modeling approach and application to a Florida case study". *Nat Haz,* 59, 1619-1634. https://doi.org/10.1007/s11069-011-9855-z

Ishibashi, H., Akiyama, M., Frangopol, D., Koshimura, S., Kojima, T., and Nanami, K. 2021. "Framework for Estimating the Risk and Resilience of Road Networks with Bridges and Embankments under both Seismic and Tsunami Hazards". *Struct Infrastruct Eng,* 17(4), 494-514. https://doi.org/10.1080/15732479.2020.1843503

Johnson, B., Chalishazar, V., Cotilla-Sanchez, E., and Brekken, T. 2020. "A Monte Carlo methodology for earthquake impact analysis on the electrical grid". *Electr Pow Syst Res,* 184. https://doi.org/10.1016/j.epsr.2020.106332

Kameshwar, S., Cox, D., Barbosa, A., Farokhnia, K., Park, H., Alam, M., and van de Lindt, J. 2019. "Probabilistic decision-support framework for community resilience: Incorporating multi-hazards, infrastructure interdependencies, and resilience goals in a Bayesian network". *Reliab Eng Syst Safe,* 191. https://doi.org/10.1016/j.ress.2019.106568

Kappes, M., Keiler, M., von Elverfeldt, and Glade, T. 2012. "Challenges of analyzing multi-hazard risk: a review". *Nat Haz,* 64, 1925-1958. https://doi.org/10.1007/s11069-012-0294-2

Logan, T, and Guikema, S. (2020). Reframing Resilience: Equitable Access to Essential Services. *Risk Analysis,* 40(8), 1538-1553. https://doi.org/10.1111/risa.13492

Madin, I., Burns, W., and McConnell, V. 2013. "Ground motion, ground deformation, tsunami inundation, coseismic subsidence, and damage potential maps for the 2012 Oregon Resilience Plan for Cascadia Subduction Zone Earthquakes". DOGAMI Open File Report O-13-06. Portland, Oregon

Martin, W., and McGuckin, N. 1998. "Travel Estimation Techniques for Urban Planning; Vol. 365". National Academy Press, Washington, DC.

National Institute of Standards and Technology (NIST). 2016. "Community resilience planning guide for buildings and infrastructure systems – Volume 1". http://dx.doi.org/10.6028/NIST.SP.1190v1. Washington, DC.

New York City Emergency Management. 2019. "NYC's Risk Landscape: A Guide to Hazard Mitigation". New York, New York.

Omer, M., Mostashari, A., and Nilchiani, R. 2011. "Measuring the Resiliency of the Manhattan Points of Entry in the Face of Severe Disruption". *Am J. Appl Sci,* 4(1), 153-161. https://doi.org/10.3844/ajeassp.2011.153.161

Omer, M., Mostashari, A., and Nilchiani, R. 2013. "Assessing Resilience in a Regional Road-based Transportation Network". *Int. J. Ind Syst Eng,* 13(4), 389-408. https://doi.org/10.1504/IJISE.2013.052605

Ouyang, M. 2014. "Review on modeling and simulation of interdependent critical infrastructure systems". *Reliab Eng Syst Safe,* 121, 43-60. https://doi.org/10.1016/j.ress.2013.06.040

Ouyang, M., and Dueñas-Osorio, L. 2014. "Multi-dimensional hurricane resilience assessment of electric power systems". *Struct Saf,* 48, 15-24. https://doi.org/10.1016/j.strusafe.2014.01.001

Oregon Seismic Safety Policy Advisory Commission (OSSPAC). 2013. "The Oregon Resilience Plan: Reducing Risk and Improving Recovery for the next Cascadia Subduction Earthquake and Tsunami". Salem, Oregon

Park, H., Cox, D., Alam, M., and Barbosa, A. 2017. "Probabilistic Seismic and Tsunami Hazard Analysis Conditioned on a Megathrust Rupture of the Cascadia Subduction Zone". *Front. Built Environ,* 3(32). https://doi.org/10.3389/fbuil.2017.00032

Park, H., Alam, M., Cox, D., Barbosa, A., and van de Lindt, J. 2019. "Probabilistic seismic and tsunami damage analysis (PSTDA) of the Cascadia Subduction Zone applied to Seaside, Oregon". *Int. J. Disaster Risk Reduct,* 35. https://doi.org/10.1016/j.ijdrr.2019.101076

Priest, G., Witter, R., Zhang, J., Wang, K., Goldfinger, C., Stimely, L., English, J., Pickner, S., Hughes, K., Wille, T., Smith, R., and McConnell, V. 2013. "Tsunami inundation scenarios for Oregon". DOGAMI Open File Report O-13-19. Portland, Oregon.

San Francisco Planning & Urban Research Association (SPUR). 2009. "The Resilient City: Defining what San Francisco needs from its Seismic Mitigation Policies". San Francisco, CA.

Sanderson, D., Kameshwar, S., Rosenheim, N., and Cox, D. 2021. "Deaggregation of multi-hazard damages, losses, risks, and connectivity: an application to the joint seismic-tsunami hazard at Seaside, Oregon". *Nat Haz* 109(21), 1821-1847. https://doi.org/10.1007/s11069-021-04900-9

Shiraki, N., Shinozuka, M., Moore, J., Chang, S., Kameda, H., and Tanaka, S. 2007. "System Risk Curves: Probabilistic Performance Scenarios for Highway Networks Subject to Earthquake Damage". *J. Infrastruct Syst,* 13(1), 43-54. https://doi.org/10.1061/(ASCE)1076-0342(2007)13:1(43)

Sun, W., Bocchini, P., and Davison, B. 2018. "Resilience Metrics and Measurement Methods for Transportation Infrastructure: The State of the Art". *Sust Res Infrastruct*, 5(3). https://doi.org/10.1080/23789689.2018.1448663

Thacker, S., Pant, R., and Hall, J. 2017. "System-of-systems formulation and disruption analysis for multi-scale critical national infrastructures". *Reliab Eng Syst Safe*, 167, 30-41. https://doi.org/10.1016/j.ress.2017.04.023

U.S. Census Bureau. 2019. Table DP05: ACS Demographic and Housing Estimates. Retrieved from https://data.census.gov/cedsci/

Wang, W., and van de Lindt, J. 2021. "Quantitative modeling of residential building disaster recovery and effects of pre- and post-event policies". *Int. J. Disaster Risk Reduct,* 59. https://doi.org/10.1016/j.ijdrr.2021.102259

Wu, J., Deng, H., Tan, Y., and Zhu, D. 2007. "Vulnerability of complex networks under intentional attack with incomplete information". *J Phys A-Math Theor*, 40, 2665-2671. https://doi.org/10.1088/1751-8113/40/11/005

Yang, T., Moehle, J., Stojadinovic, B., and Der Kiureghian, A. 2009. "Seismic Performance Evaluation of Facilities: Methodology and Implementation". *J. Struct. Eng*., 135(10), 1146-1154. https://doi.org/10.1061/(ASCE)0733-9445(2009)135:10(1146)

Zhang, N., and Alipour, A. 2020. "Multi-scale robustness model for highway networks under flood events". *Transp Res Part D Transp Environ,* 83. https://doi.org/10.1016/j.trd.2020.102281

Zhang, Q., Northridge, M., Jin, Z., and Metcalf, S. 2018. "Modeling accessibility of screening and treatment facilities for older adults using transportation networks". *Appl Geogr,* 93, 64-75. https://doi.org/10.1016/j.apgeog.2018.02.013

Zhang, X., Miller-Hooks, E., and Denny, K. 2015. "Assessing the Role of Network Topology in the Transportation Network Resilience". *J Transp Geogr,* 46, 35-45. https://doi.org/10.1016/j.jtrangeo.2015.05.006

Zou, Q., and Chen, S. 2020. "Resilience Modeling of Interdependent Traffic-Electric Power System Subject to Hurricanes". *J. Infrastruct Syst,* 26(1): 04019034. https://doi.org/10.1061/(ASCE)IS.1943-555X.0000524